ACS Photonics

Article

pubs.acs.org/journal/apchd5

Multifunctionality of Giant and Long-Lasting Persistent Photoconductivity: Semiconductor−Conductor Transition in Graphene Nanosheets and Amorphous InGaZnO Hybrids

Min-Kun Dai,[†] Yi-Rou Liou,[†] Jan-Tien Lian,[‡] Tai-Yuan Lin,[*,‡] and Yang-Fang Chen[*,†]

[†]Department of Physics, National Taiwan University, Taipei 106, Taiwan

[‡]Institute of Optoelectronic Sciences, National Taiwan Ocean University, Keelung 202, Taiwan

ABSTRACT: Composite materials can play a decisive role to reveal novel physical properties and enable to advance new generation technologies. Here, we discover that phototransistors based on the integration of two-dimensional graphene nanosheets (GNSs) and amorphous indium−gallium−zinc−oxide (a-IGZO) semiconductors exhibit a giant photo-to-dark current ratio and long-lasting persistent photoconductivity (PPC). Under the illumination of UV light (350 nm) at 50 mW/cm^2, a photo-to-dark current ratio up to 2.0×10^7 was obtained, which is about 3 orders of magnitude higher than its pure a-IGZO device counterpart. Moreover, the GNSs/a-IGZO phototransistor possesses an enduring lifetime up to years for the recovery of the transfer characteristics after switching off the UV light. The giant and long-lasting PPC leads GNSs/a-IGZO to become an excellent conductor with conductivity much better than indium tin oxide. The observed unique features represent a semiconductor−conductor transition. In addition to next generation flat, flexible, and display, it can open up a wide variety of application, such as transparent electrodes for optoelectronic devices, optical memory, and light harvesting for energy storage. As an example, we demonstrated the operation of optical memory devices, which may lead to the novel application of holographic storage. Our results shown here therefore provide an outstanding new route for the future development of solution-processable semiconducting optoelectronic devices.

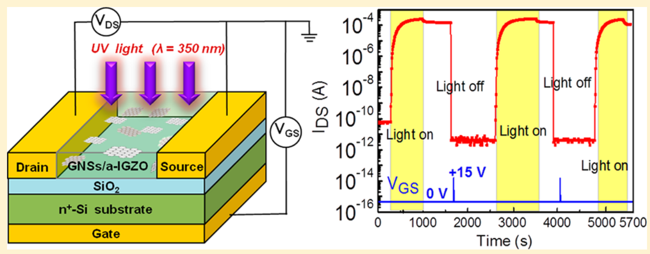

KEYWORDS: *semiconductor-conductor transition, graphene nanosheets (GNSs), amorphous indium−gallium−zinc oxide (a-IGZO), phototransistor, optical memory*

Due to the coupling among constituent materials, hybrid composites enable to possess exceptional properties and multifunctionality, which cannot be found in single component. As a result, their applications can be expanded to a wide range of fields. Recently, amorphous oxide semiconductor (AOS) have created a new area of electronics and optoelectronic devices.[1,2] Among the various AOS types, amorphous indium−gallium−zinc oxide (a-IGZO) thin-film transistors (TFTs) have been considered to be one of the most promising candidates for next-generation flat, flexible, and transparent display devices, mainly owing to their high electron mobility, optical transparency, chemical stability, and processing versatility.[3,4] Replacing TFTs made of hydrogenated amorphous silicon (a-Si: H) with transparent a-IGZO TFTs can significantly boost the aperture ratio of pixels, reduce the power, and simplify device fabrication.[5,6] For system-on-panel (SoP) applications, IGZO-based nonvolatile memory (NVM) is required, and many research teams are actively pursuing related devices.[7−9] Besides, the IGZO-based TFTs have been utilized in phototransistors and photosensors due to their high sensitivity to light, mobility, and on/off ratio for integrated circuits.[10,11] With the additional terminal, light memory devices based on IGZO and AOS phototransistor can be realized with the special optical programming and electrical erasing processes.[12,13] To ensure the application in nonvolatile memories such as flash memory, a long retention time is one of the most important criteria for phototransistor memory devices.[14] Additionally, the decay time of persistent photocurrent (PPC; or retention time as the memory device) should be as long as possible. Furthermore, a large ON/OFF current ratio is advantageous to the electronic logic and memory devices for the less influence of the noise on the signal. Room temperature PPC has been observed in a variety of II−VI[15] and III−V[16,17] semiconductors, including GaN-related semicondutors.[18−20] Even though the increment of conductivity for the PPC in the above-mentioned traditional semiconductors does not exceed more than 1 order of magnitude, nonetheless, long-lasting PPC with increased conductivity over two and 5 orders of magnitude at room temperature in strontium titanate ($SrTiO_3$) single crystal[21] and $SrTiO_3/LaAlO_3$ interfaces[22] were recently reported, respectively.

In yet another emerging substance, a wide variety of carbon-based nanomaterials has been extensively studied, including graphene nanosheets (GNSs), carbon nanotubes (CNTs),

Received: February 25, 2015
Published: July 1, 2015

DOI: 10.1021/acsphotonics.5b00084
ACS Photonics 2015, 2, 1057−1064

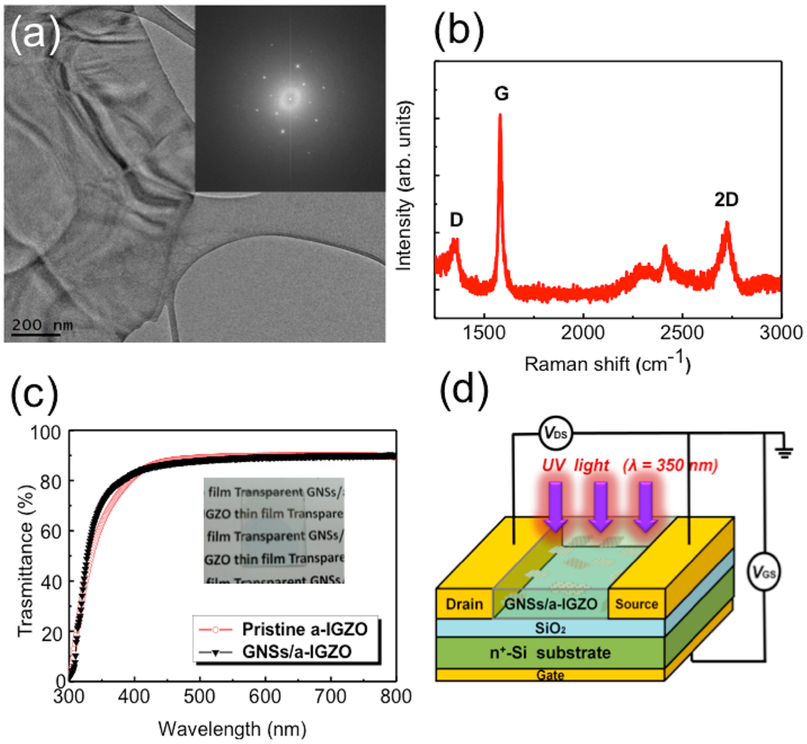

Figure 1. (a) High-resolution TEM images of graphene nanosheets showing the mixture of a few graphene layers. The inset shows the corresponding selected area electron diffraction (SAED) pattern. The scale bar is 200 nm. (b) Typical Raman spectrum of multilayer graphene with a 532 nm excitation laser wavelength. (c) Transmittance spectrum of spin-coated GNSs/a-IGZOthin films on a glass substrate. (d) Schematic representation of solution-based GNSs/a-IGZO phototransistors.

nanoribbons, nanodiamonds, fullerenes, carbon nano-onions, and other carbonaceous nanostructures.[23,24] The integration of semiconductors and graphene-based nanomaterials has been found to form novel hybrid nanocomposites with unprecedented physical phenomena, toward a wide range of application, such as solar cells, transistors, and memories.[25−29] Especially, the solution-exfoliation methods have been developed to prepare the high-quality GNSs dispersions, which are viable for fabricating graphene-based composites by spray coating, vacuum filtration or drop casting.[23,24,30] In our previous study,[31] for instance, by blending a-IGZO sol−gel solution with the exfoliated GNSs solution, solution-processed GNSs/a-IGZO composite films have been used to obtain high-performance TFTs, in which the transport resistance can be significantly reduced due to the excellent conductivity via the network of GNSs. Since the PPC is believed to occur by virtue of spatial separation of photogenerated electrons and holes. Such composites are naturally suitable for the creation of PPC, because the photogenerated charge carriers in IGZO could be transferred to graphene via the existence of electrostatic filed across the graphene/IGZO interfaces.

In this study, GNSs and a-IGZO materials have been synthesized, and the phototransistors based on GNSs/a-IGZO composites have been fabricated and investigated. It is discovered that the phototransistors exhibit several intriguing characteristics, including enhanced carrier mobility, wide memory window, colossal photo-to-dark current ratio, and extremely long-lifetime PPC. With the assistance of GNSs in the a-IGZO matrix, the photo-to-dark current ratio of the GNSs/a-IGZO phototransistors can be enhanced by up to 2.0 $\times$ 10^7 under UV light illumination (350 nm) of 50 mW/cm^2, which is about 3 orders of magnitude greater than that of its pure a-IGZO TFT counterpart. In addition, the photocurrent persists for several days up to years with highly stable retention characteristics after turning off the light. Notably, it is far beyond the recently reported value for the PPC observed in strontium titanate crystal (as claimed for several days).[21] The long-lasting large PPC leads GNSs/a-IGZO to become a good conductor with conductivity much better than indium tin oxide. On the basis of the discovered giant and long-lasting PPC, we demonstrated the operation of an optical memory device, which may lead to the development of holographic storage.[21,32] Moreover, the discovered new features represent an alternative route for semiconductor-conductor transition, which may open up a wide variety of application, such as high sensitive photodetectors, transparent electrodes for solar cells and light emitting diodes, and a new type of light harvesting for energy storage. Therefore, our approach could provide a simple and feasible way to advance solution-processable semiconductor-graphene composite devices with multifunctionalities for a wide range of application.

RESULTS

Characterization of the GNSs/a-IGZO Composites. To investigate the morphology and quality of the solution-based GNSs prepared by graphite dispersion in a surfactant−water solution, we first characterized GNSs by transmission electron microscopy (TEM) and Raman spectroscopy. Figure 1a shows the high-resolution TEM images and the selected area electron diffraction (SAED) patterns of the GNSs deposited on a specific copper grid. The TEM image shows that the dispersed phase consists of small graphene flakes. The GNSs exhibit the typical wrinkled structure with corrugation and scrolling that is intrinsic to graphene. The well-defined diffraction spots in the

DOI: 10.1021/acsphotonics.5b00084
ACS Photonics 2015, 2, 1057−1064

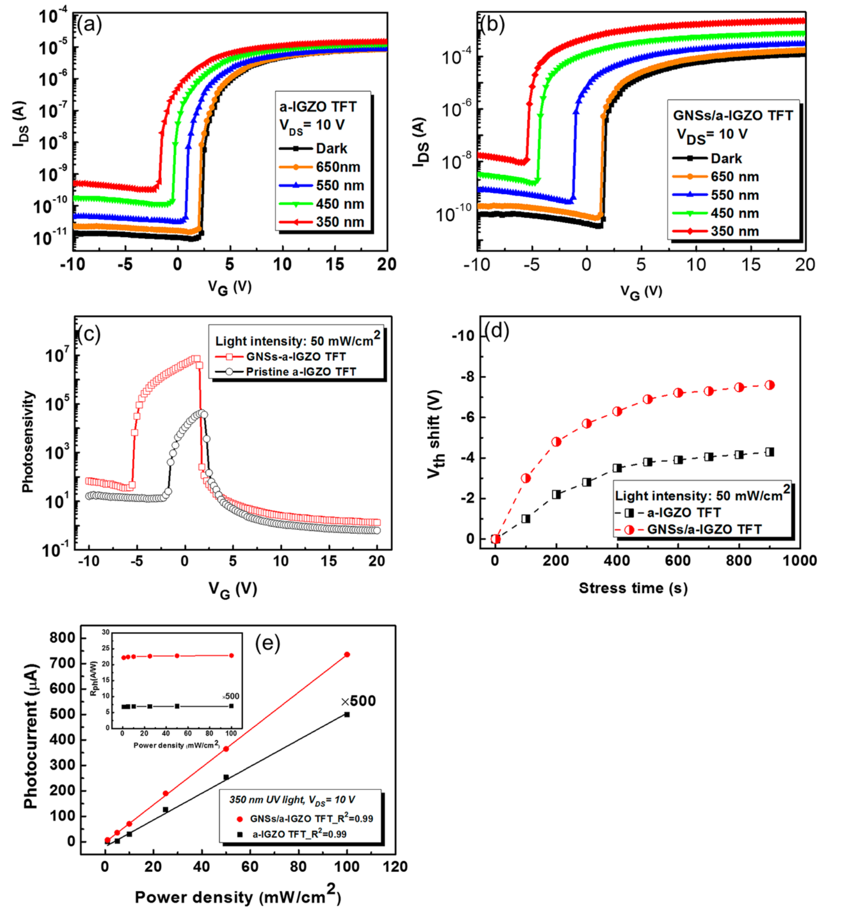

Figure 2. Transfer characteristics of (a) a-IGZO and (b) GNSs/a-IGZO TFTs before and after UV illumination. The photoexcitation measurement is operated after 10 min with a UV light illumination intensity of 50 mW/cm^2. (c) Gate-voltage dependent photo-to-dark current ratio at V_{DS} = 10 V. (d) Temporal evolution of the threshold-voltage shift for a-IGZO and GNSs/a-IGZO devices under UV illumination. (e) Photocurrent of the a-IGZO and the GNSs/a-IGZO UV phototransistors as a function of incident optical power of 350 nm UV light at 10 V bias. Inset: Photoresponse of the a-IGZO and the GNSs/a-IGZO UV phototransistors.

SAED patterns confirm the excellent crystalline structure of the graphene films and that they consist of stacks of few-layer sheets. In Figure 1b, Raman spectroscopy was also used to characterize the as-prepared GNSs, which shows the three main peaks: the D-band (1360 cm^{-1}), G-band (1580 cm^{-1}), and 2D-band (2722 cm^{-1}). The D-band, known as the disorder band or defect band, is due to the breathing mode of sp^2 carbon rings and requires a defect for its activation.[35] The G-band corresponds to the planar configuration of sp^2-bonded carbon that constitutes graphene. The 2D-band is the most prominent feature in the Raman spectrum of the underlying graphene. The relative intensity ratio I_{2D}/I_G is approximately 0.40, which suggests that the as-prepared GNSs in the surfactant/water solutions contain a random distribution of few-layer grapheme.[36,37] Figure 1c shows the transmittance spectrum in the 300−900 nm wavelength range for both the a-IGZO and GNSs/a-IGZO films. It is observed that both films are highly transparent in the visible range (400−700 nm) with a transparency greater than 80%. The inset in Figure 1c shows a photographic image of the hybrid GNSs/a-IGZO film on quartz, clearly illustrating the transparency of the film.

Photoinduced Effects of the GNSs/a-IGZO Hybrid TFTs and a-IGZO TFTs. The layout of the devices used in the present study is based on a bottom-gate transistor structure, as shown schematically in Figure 1d. The photoinduced effects on the electrical characteristics of the a-IGZO TFT and GNSs/a-IGZO TFTs were explored by illumination of a variety of light onto the top of devices with a power density of 50 mW/cm^2. The transfer characteristics of the TFTs were taken at room temperature for gate voltages, V_G, varying from −10 to 20 V under a fixed source−drain voltage, V_{DS}, of 10 V. Figure 2a,b shows the transfer characteristics measured under dark and light illumination at various wavelengths (λ = 650 to 350 nm) on the a-IGZO and GNSs/a-IGZO TFTs, respectively. The values of the field-effect mobility in the saturation region μ_{sat} were determined by

$$I_{DS,sat} = \frac{W}{2L}\mu_{sat}C_i(V_G - V_{th})^2 \tag{1}$$

where W is the channel width, L is the channel length, and C_i is the capacitance per unit area of the gate dielectric. In the dark, the a-IGZO TFTs have a value for μ_{sat} of 0.85 cm^2/V·s, a threshold voltage V_{th} of 2.23 V, and a subthreshold swing (SS) of 0.87 V/decade. In contrast, the GNSs/a-IGZO TFT exhibits superior characteristics with a value for μ_{sat} of 24.2 cm^2/V·s, V_{th} of 1.52 V, and SS of 0.62 V/decade. The TFT characteristics vary substantially with the oxide semiconductor compositions and the details of the process used for the various devices. Oxide semiconductor TFTs in the IGZO family, processed from solution by the sol−gel method result in TFTs with a wide range of mobility. The characteristics values for the GNSs/a-IGZO TFTs of our work here are superior to that of

DOI: 10.1021/acsphotonics.5b00084
ACS Photonics 2015, 2, 1057−1064

Table 1. Extracted Electrical Parameters of a-IGZO and a-IGZO/GNSs TFTs with and without Light Illumination

active layer	measurement condition	threshold voltage (V)	mobility($cm^2/V{\cdot}s$)	subthreshold swing (V/dec)	on/off current ratio
a-IGZO	dark	2.23	0.85	0.87	1.02×10^6
	illumination	−1.78	1.13	0.91	3.58×10^4
GNSs/a-IGZO	dark	1.52	24.2	0.62	3.43×10^6
	illumination	−5.70	36.5	0.70	2.54×10^5

the previously reported solution-based IGZO/single-walled carbon nanotubes blend thin film transistors,[38] as well as to the values for the recently reported IGZO transistors that were deposited using solution-based processes by optimized conditions,[39] and are comparable to the values for sputtered *a*-IGZO TFTs.[40] Both of the TFTs exhibit excellent on/off current ratios in the range of 10^6. It is observed that the GNSs/a-IGZO TFTs possess better performance than the pristine a-IGZO TFTs in the dark. As reported in our previous study,[31] GNSs play an important role for greatly reducing the effective channel resistance of carrier transport in the a-IGZO matrix. Upon light illumination, both the a-IGZO TFTs and GNSs/a-IGZO TFTs showed the increase in source−drain current, and the negative shift in the threshold voltage (ΔV_{th}) decreases with the wavelength of the illumination light. Prominent variations in photocurrent and threshold voltage were observed for the incident illumination with wavelength of 450 nm, in contrast to the very small changes for the wavelengths longer than 650 nm. What is more, a remarkable shift in the threshold voltage was observed in the GNSs/a-IGZO TFTs as the illuminated wavelength is set at 350 nm, whose energy is above the band gap of a-IGZO. For the shedding of 350 nm UV light, the source−drain current of the a-IGZO TFTs increases from 1.66×10^{-11} Å to 5.14×10^{-7} Å at $V_G = 0$ V. The photo-to-dark current ratio, S_{ph}, of the TFTs can be defined as follows:

$$S_{ph} = \frac{I_{ph}}{I_{dark}} = \frac{I_{ill} - I_{dark}}{I_{dark}} \tag{2}$$

where I_{ph} is the photocurrent, which is equal to the difference between the current under illumination (I_{ill}) and under dark (I_{dark}) at the same gate and drain voltages. Thus, a high photo-to-dark current ratio for the a-IGZO TFTs is 3.1×10^4. Interestingly, we observed a more pronounced result for the GNSs/a-IGZO TFTs, in which the source−drain current increases from 3.82×10^{-11} to 7.56×10^{-4} A. The photo-to-dark current ratio is as high as 2.0×10^7, which is about 3 orders of magnitude higher than that of the a-IGZO TFT devices without the GNSs inserted. Our results demonstrate that the GNSs/a-IGZO blend is highly photoresponsive to the light and could be a good candidate for an ultraviolet photodetector. The corresponding electrical parameters of the a-IGZO and GNSs/a-IGZO TFTs are further summarized in Table 1. Figure 2c shows the photo-to-dark current ratio as a function of V_G for the pristine a-IGZO and GNSs/a-IGZO TFTs with a fixed illumination intensity. It is clear that the photo-to-dark current ratio depends strongly on the applied gate bias. For the GNSs/a-IGZO TFTs, a maximum photo-to-dark current ratio up to 10^7 is observed for a gate bias of 1 V with UV light (50 mW/cm^2) illumination, whereas the minimum photo-to-dark current ratio is 1.33 at $V_G = 20$ V. These results indicate that the devices possess a good gate-tuning effect and high photo-to-dark current ratio, even at low illumination intensity; thus, it is especially suitable for the development of UV light detector applications.

In amorphous-oxide semiconductors, there exist high-density subgap states originating from the oxygen vacancies close to the valence-band maximum (VBM) and tail states, which is the origin of the significant response to electrical bias and illumination stress.[41,42] According to Lee et al., the negative shift in the threshold voltage (ΔV_{th}) of Hf−In−Zn−O (HIZO) TFTs under light stress was explained by light-enhanced hole trapping.[43] Furthermore, Görrn et al. also attributed the negative ΔV_{th} in unpassivated Zn−Sn−O (ZTO) TFTs to the persistent photoconductivity induced by surface effects.[44] Here, we investigate the TFT stability dependence on light-induced effects. Comparing Figure 2a and b, with focus on 350 nm UV light, the GNSs/a-IGZO TFTs exhibit a remarkable shift in V_{th}, with a negative ΔV_{th} of 7.22 V for GNSs/a-IGZO TFTs, which is much larger than that of 4.01 V for a-IGZO TFTs. The large negative ΔV_{th} relative to the fresh state indicates that GNSs/a-IGZO TFTs can provide a large memory window, which in turn produces a large margin of read-out voltage for nonvolatile memory operations. The photoinduced memory window in a-IGZO TFTs can be well understood because photon-assisted hole trapping followed by ionization of oxygen vacancy (V_O) sites occurs at the a-IGZO/gate-insulator interface and at a-IGZO bulk defects.[12] Figure 2d shows the memory window as a function of time during the 15 min UV light illumination for the a-IGZO and GNSs/a-IGZO TFTs. It is clear that the light-stress-induced ΔV_{th} (memory window) is accelerated in the GNSs/a-IGZO devices. According to the above results, the insertion of GNSs in a-IGZO matrix does not only greatly enhance the photo-to-dark current ratio but also significantly increases the memory window, ΔV_{th}, for memory device operations. The device performance was further examined on the amount of current increase under illumination (compared with the current in dark at $V_{DS} = 10$ V) against the power of the incident UV light.[45] Figure 2e shows the photocurrent and photoresponse of the a-IGZO and the GNSs/a-IGZO UV phototransistors under various illumination intensities of 350 nm UV light. For both a-IGZO and GNSs/a-IGZO TFTs, the calibration curves showed a strong linear relationship with a correlation coefficient, R^2 of 0.99. The fact that the photocurrent increases linearly with illumination light intensity, which is consistent with charge carrier photo-generation efficiency proportional to the absorbed photon flux. It indicates that our GNSs/a-IGZO based TFTs could work potentially as a UV phototransistors. In consequence, our results do illustrate that hybrid composites are able to possess exceptional properties and multifunctionality,[46,47] which can not be found in single component.

Spectral Responsivities and Persistent Photoconduction of the Phototransistors. In Figure 3a, we plot the measured spectral responsivities of the fabricated devices. The photoresponsivity, R_{ph}, of the TFTs can be defined as follows:

$$R_{ph} = \frac{I_p}{P_i} \tag{3}$$

DOI: 10.1021/acsphotonics.5b00084
ACS Photonics 2015, 2, 1057−1064

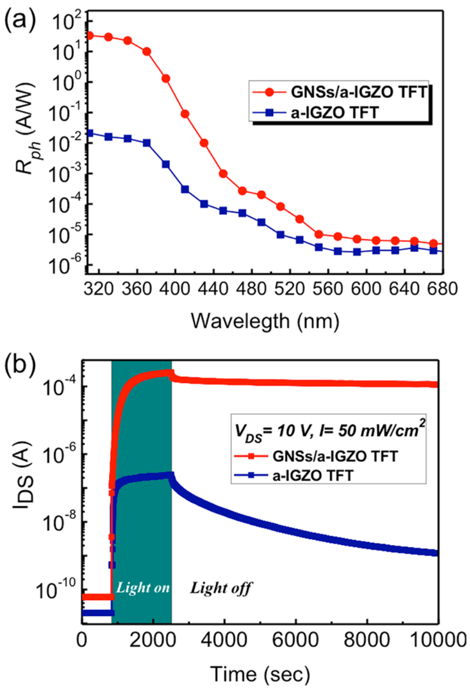

Figure 3. (a) Spectral response measured from a-IGZO and GNSs/a-IGZO TFTs with $V_G = 0$ V. (b) Typical time response of the source−drain current with zero gate bias and a light pulse (50 mW/cm^2) for a-IGZO TFTs and GNSs/a-IGZO TFTs.

where P_i is the incident light intensity and I_p is the photocurrent. All devices exhibit a sharp cutoff at 370 nm, which corresponds to the band gap of a-IGZO. With an incident light wavelength of 350 nm, pristine a-IGZO phototransistors yield a value for R_{ph} of 0.014 A/W. In contrast, a much higher R_{ph} of 22.8 A/W can be obtained for the GNSs/a-IGZO TFTs. Notably, R_{ph} of GNSs/a-IGZO nanocomposite phototransistors exhibits much better performance than other a-IGZO-based deep-UV phototransistors with the specific high-*k* dielectric.[10,48] Figure 3b shows the rise of the channel photocurrent upon continuous illumination of UV light (350 nm) and the photocurrent decay after removal of incident light in the GNSs/a-IGZO and a-IGZO TFTs, which shows a remarkable PPC effect after turning off the incident light. The slow dynamics of the photocurrent rise and decay times presented here are similar to the corresponding values observed in phototransistors based on amorphous oxide semiconductors.[12,13] Quite remarkably, it can be seen that the PPC becomes much more pronounced as GNSs are incorporated into the devices. On the basis of the mathematical extrapolation of our experimental result sustaining the high photo-to-dark current ratio (~10^7) yet at the measuring time of 10^4 s, the pronounced persistent photocurrent of the GNSs/a-IGZO TFTs can be potentially maintained up to years. Obviously, this gigantic persistent photocurrent in GNSs/a-IGZO TFTs far exceeds all previously reported values.[12,15,19,21] The giant and ultralong PPC leads GNSs/a-IGZO composite to become an excellent conductor. In our present case, the conductivity ($5 \times 10^{-2}\ \Omega^{-1}\ cm^{-1}$) is more than 1 order of magnitude larger than that of indium tin oxide. The long-lasting photocurrent in GNSs/a-IGZO TFTs can definitely provide a great deal of potential application by precise control over the ON and OFF states, including optical memory, transparent electrodes for solar cells and light emitting diodes, and light harvesting for energy storage. Thus, the GNSs/a-IGZO composite we have demonstrated here could open up a new route to create semiconductor-conductor transition and generate high performance optoelectronic devices based on the PPC effect.

DISCUSSION

The underlying mechanism of the observed enhancement in photo-to-dark current ratio and persistent photocurrent can be explained by using the proposed model and band diagram schematically depicted in Figure 4a and b, respectively. Figure 4a illustrates the effects of UV light illumination in the IGZO active layer. Multiple electron−hole pairs were generated under UV light illumination when the photon energy is larger than the band gap of the a-IGZO thin film owing to band-to-band excitation, which results in the photoconductivity in semiconductors. Additionally, electrons can also be generated as a result of excitation from the deep-level traps to the conduction band of a-IGZO. For example, oxygen vacancies with doubly charged V_O^{2+} or singly charged V_O^{+} can be generated, which provides free electrons and interstitial O atoms in the system.[10,49,50] After turning off the light illumination, the

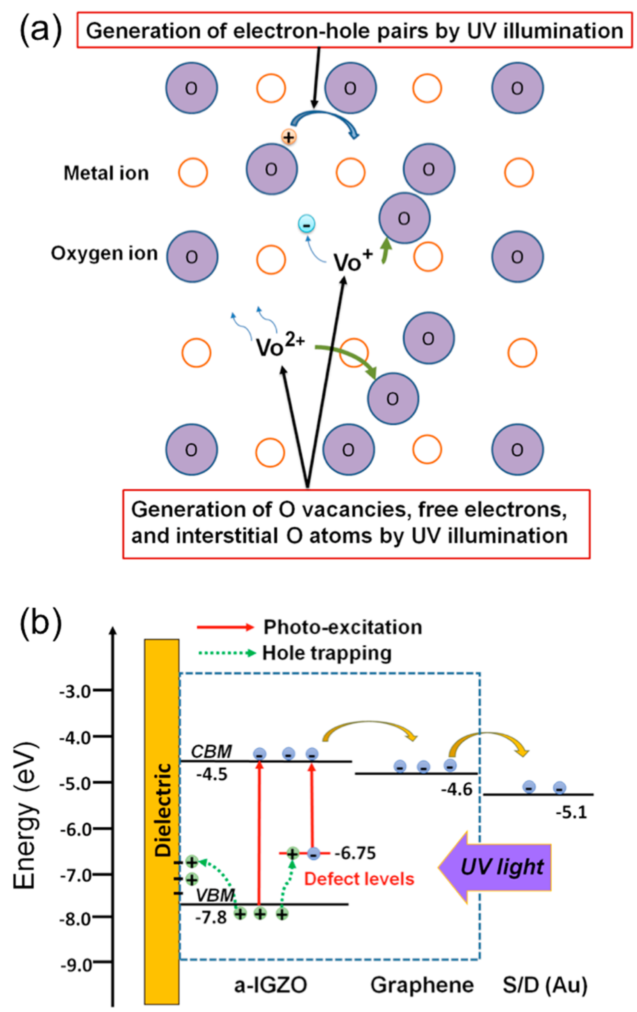

Figure 4. (a) Qualitative description of UV illumination effects. UV illumination induces the generation of O vacancies, free electrons, and interstitial O atoms along with electron−hole pairs. (b) Band diagram of a GNSs/a-IGZOTFT and the transport of photogenerated electrons and holes under UV light illumination.

DOI: 10.1021/acsphotonics.5b00084
ACS Photonics 2015, 2, 1057−1064

recovery of the off-current in the a-IGZO TFTs arises from the recombination of electron−hole pairs, resulting in the reduction of free electrons in the a-IGZO layer. However, the photogenerated positive charges in the metal-oxide semiconductor tend to be localized in the V_O defects of the a-IGZO matrix and the interface trap sites between the dielectric layer and a-IGZO.[37,51−53] As a result, it prevents the recombination of photogenerated electron−hole pairs, prolongs the existence of photocurrent, and results in a V_{th} shift.

As GNSs are introduced into a-IGZO matrix, the light-response phenomena of the phototransistors change drastically, as shown in Figures 2 and 3. Apparently, the ultrahigh photo-to-dark current ratio and very slow recovery of the off-current for the GNSs/a-IGZO TFTs can be attributed to the important role played by GNSs and understood on the basis of the energy diagram depicted in Figure 4b. Under UV light illumination, electron−hole pairs are generated by photoexcitation in the device. The dissociation of photogenerated electron−hole pairs with the assistance of band alignment at the GNSs/a-IGZO interface results in a better migration of the photogenerated electrons from the a-IGZO matrix to the GNSs, thus, reducing the recombination. In addition, the high conductivity of the GNSs assists in producing the higher carrier mobility in the device.[31] Therefore, it is expected that the GNSs/a-IGZO TFTs have superior photo-to-dark current ratio when compared with the pristine a-IGZO TFTs. Because the recombination probability of the photogenerated electron−hole pairs is significantly reduced, holes now have a greater probability of being trapped by the defects in a-IGZO and at the a-IGZO/SiO_2 interface. These highly localized holes cannot easily escape from the trapping centers and recombine with free electrons.[41] As a consequence, this leads to the very long recovery time of the photocurrent, the large ΔV_{th}, and the much more pronounced photoconductivity after turning off the light illumination. Conversely, the PPC can be eliminated by releasing the trapped carriers through recombination with carriers of the opposite sign. For the current case, the trapped holes can be released by a positive gate bias in the three terminal a-IGZO/SiO_2 TFT device. As the trapped holes escape back to the channel, the accelerated recovery of the photocurrent is predictable due to the enhanced electron−hole recombination.

Finally, in order to illustrate the potential application, we demonstrate the operation of optical memory characteristics based on the everlasting lifetime of the persistent photocurrent as shown in Figure 5. It is interesting to note that a multibit programmable optoelectronic ZnO based nanowire memory utilizing the photoinduced charged defects as surface trapped charges to provide the electrical memory effect has been recently demonstrated.[54] For the current case, after turning off the light illumination, I_{DS} slightly decreases and eventually remains at a metastable state owing to the spatial separation of photogenerated charge carriers. At a specific moment, a single positive pulse of the gate bias (V_G = +15 V, 600 ms) is applied to accelerate the recovery. Based on the positively pulsed gate bias, the trapped holes are released and quickly recombine with electrons, thereby enhancing the recombination.[13,53] Thus, the adverse effect of PPC can be overcome and the GNSs/a-IGZO device can be effectively reset to the original dark state with a subsecond time decay response. The red line in Figure 5 records the output currents I_{DS} during the memory cycles. Based on the result that the photocurrent increases linearly with illumination light intensity as shown in Figure 5, the required

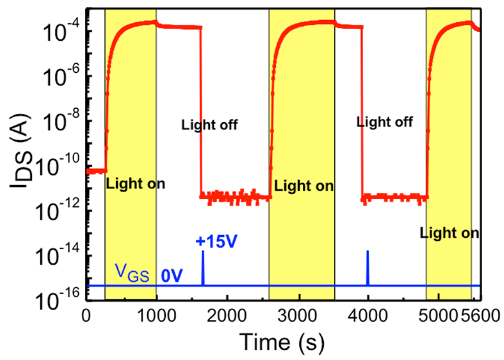

Figure 5. Cycling responses of the optical programming and electrical erasing of a typical GNSs/a-IGZO TFTs device. The light was turned on (yellow region) and turned off (white region) for the programming and retention operations. A short positive gate-voltage pulse (+15 V, 600 ms) was applied at 1620 and 3910 s to erase the memory effect.

optical writing energy is around 64 μJ/bit if two-orders magnitude of on−off ratio is assumed for the writing process, which is smaller than that of the thin film memory device using the PPC effects.[55] On the basis of this mode of operation, we could not only program the GNSs/a-IGZO device optically and electrically erase it repeatedly, but we could also ensure the enduring retention time due to the gigantic persistent photocurrent.

■ SUMMARY

Summarizing our experimental findings, we have demonstrated phototransistors with giant photo-to-dark current ratio and long-lasting photoconduction based on a novel nanocomposite consisting of amorphous indium−gallium−zinc oxide and GNSs via a sol−gel technique. As GNSs were introduced into the a-IGZO matrix, the electron mobility was enhanced by more than 10 times, and the photo-to-dark current ratio reached up to 2.0×10^7 under the UV light illumination of 50 mW/cm^2, which is larger than that of pristine a-IGZO TFTs. In addition, it was found that the photocurrent can persist for several days up to years with insignificant degradation. The underlying mechanism can be understood by the transfer of photoinduced electrons from the a-IGZO matrix to the GNSs with the assistance of the band alignment between a-IGZO and GNSs and the high carrier mobility of the GNSs. We further suggest that the electron transfer from the a-IGZO matrix to the GNSs provides an excellent opportunity for photoinduced holes trapped by defect sites in the a-IGZO matrix and at the interface between the dielectric layer and a-IGZO, which gives rise to the gigantic persistent photocurrent. The newly developed GNSs/a-IGZO TFTs therefore possess several unique properties compared with pristine a-IGZO TFTs. On the basis of the observed persistent photocurrent, the operation of optical memory devices has been demonstrated. Thus, our results enable to advance solution-processable AOS devices with improved functionalities for a broad range of practical applications including high-performance flat, flexible, and fully transparent display devices as well as optical memory devices for holographic storage. It is stressed that, the unique features discovered here represent an eminent semiconductor-conductor transition, which may open up an alternative route for the creation of composite materials with multifunctionality, including ultrahigh sensitive photodetector, transparent con-

DOI: 10.1021/acsphotonics.5b00084
ACS Photonics 2015, 2, 1057−1064

ducting electrodes for solar cells and light emitting devices, and a new type of light harvesting for energy storage.

EXPERIMENTAL METHODS

Synthesis of a-IGZO and GNSs/a-IGZO Composites. The 0.01 M precursor solution for the a-IGZO sol−gel solution was prepared by dissolving indium chloride ($InCl_3$, Sigma-Aldrich Inc.), gallium chloride ($GaCl_3$, Sigma-Aldrich Inc.), and zinc chloride ($ZnCl_2$, Sigma-Aldrich Inc.) into 10 mL of ethylene glycol ($C_2H_6O_2$, Sigma-Aldrich Inc.) at 75 °C. The composition of the a-IGZO sol−gel solution was In_2O_3/Ga_2O_3/ZnO = 1:1:1 in the stoichiometric molar ratio. On the other hand, the GNSs solution was prepared by a graphite dispersion in a surfactant−water solution following a standard procedure described in the literature.[33,34] Briefly, a dispersion (~200 mL) with initial graphite concentration of 0.1 mg/mL, and surfactant (sodium dodecylbenzenesulfonate, SDBS) concentration of 0.5 mg/mL was prepared first following by the decanter centrifugation. A typical sample was prepared by dispersing graphite in the desired SDBS concentration using sonication in a sonic bath. The resulting dispersion was left to stand for ~24 h before the centrifugation. After centrifugation, the top 10 mL of the dispersion was decanted for use. For the fabrication of the GNSs/a-IGZO composite, the a-IGZO solution was blended with the exfoliated graphene solution described above and stirred at 50 °C for 1 h. The volume fraction of the GNSs in the a-IGZO matrix was 0.15 vol %.

Fabrication of a-IGZO and GNSs/a-IGZO TFTs. The layout of the GNSs/a-IGZO TFTs consisted of a bottom-gate transistor structure. A 300 nm-thick SiO_2 film was formed as the gate insulator by thermal oxidation of heavily n-doped silicon. The Au source (S) and drain (D) electrodes with a length (L) of 40 μm and a width (W) of 800 μm were formed by thermal evaporation. The composite solutions were then spun onto SiO_2 substrates to serve as the active films. For the removal of residual surfactants, the samples were annealed at 500 °C for 1 h in ambient air.

Characterization and Measurements. All electrical characteristics of the transistors were measured with a probe station system and a Keithley 4200-SCS semiconductor parameter analyzer under ambient conditions. For the photo-induced effect measurements, UV light was provided by a 250-W xenon arc lamp passed through a band-pass filter centered at a wavelength of 350 nm. The power density of the UV light was calibrated by means of neutral density filters. The Raman scattering spectra were obtained at room temperature using a Jobin Yvon LabRam-HR 800 micro-Raman spectrometer.

AUTHOR INFORMATION

Corresponding Authors

*E-mail: tylin@ntou.edu.tw. Tel: +886-2-24622192 ext. 6703. Fax: +886-2-24634360.
*E-mail: yfchen@phys.ntu.edu.tw. Tel.: +886-2-33665125. Fax: +886-2-23639984.

Notes

The authors declare no competing financial interest.

ACKNOWLEDGMENTS

This work was supported by the National Science Council and the Ministry of Education of the Republic of China.

REFERENCES

(1) Pattanasattayavong, P.; Rossbauer, S.; Thomas, S.; Labram, J. G.; Snaith, H. J.; Anthopoulos, T. D. Solution-processed dye-sensitized ZnO phototransistors with extremely high photoresponsivity. *J. Appl. Phys.* **2012**, *112*, 074507.

(2) Park, S. H. K.; Hwang, C. S.; Ryu, M.; Yang, S.; Byun, C.; Shin, J.; Lee, J. I.; Lee, K.; Oh, M. S.; Im, S. Transparent and photo-stable ZnO thin-film transistors to drive an active matrix organic-light-emitting-diode display panel. *Adv. Mater.* **2009**, *21*, 678−682.

(3) Park, J. S.; Maeng, W. J.; Kim, H. S.; Park, J. S. Review of recent developments in amorphous oxide semiconductor thin-film transistor devices. *Thin Solid Films* **2012**, *520*, 1679−1693.

(4) Lee, S. M.; Yu, C. G.; Cho, W. J.; Park, J. T. Hot carrier degradation of InGaZnO thin film transistors under light illumination at the elevated temperature. *Solid-State Electron.* **2012**, *72*, 88−92.

(5) Kamiya, T.; Nomura, K.; Hosono, H. Present status of amorphous In−Ga−Zn−O thin-film transistors. *Sci. Technol. Adv. Mater.* **2010**, *11*, 044305.

(6) Shin, J. H.; Cheong, W. S.; Hwang, C. S.; Chung, S. M. Modeling of amorphous InGaZnO thin film transistors using an empirical mobility function based on the exponential deep and tail states. *Thin Solid Films* **2012**, *520*, 3800−3802.

(7) Yoon, S. M.; Yang, S.; Byun, C. W.; Jung, S. W.; Ryu, M. K.; Park, S. H. K.; Kim, B. H.; Oh, H.; Hwang, C. S.; Yu, B. G. Nonvolatile memory thin-film transistors using an organic ferroelectric gate insulator and an oxide semiconducting channel. *Semicond. Sci. Technol.* **2011**, *26*, 034007.

(8) Su, N. C.; Wang, S. J.; Chin, A. A nonvolatile InGaZnO charge trapping engineered flash memory with good retention characteristics. *IEEE Electron Device Lett.* **2010**, *31*, 201−203.

(9) Nguyen, H. H.; Nguyen, V. D.; Trinh, T. T.; Jang, K.; Baek, K.; Raja, J.; Yi, J. Fabrication of $SiO_2/SiO_x/SiO_xN_y$ non-volatile memory with transparent amorphous indium gallium zinc oxide channels. *J. Electrochem. Soc.* **2011**, *158*, H1077−H1083.

(10) Chang, T. H.; Chiu, C. J.; Chang, S. J.; Tsai, T. Y.; Yang, T. H.; Huang, Z. D.; Weng, W. Y. Amorphous InGaZnO ultraviolet phototransistors with double-stack Ga_2O_3/SiO_2 dielectric. *Appl. Phys. Lett.* **2013**, *102*, 221104.

(11) Liu, X.; Yang, X. X.; Liu, M. J.; Tao, Z.; Dai, Q.; Wei, L.; Li, C.; Zhang, X. B.; Wang, B. P.; Nathan, A. Photo-modulated thin film transistor based on dynamic charge transfer within quantum-dots-InGaZnO interface. *Appl. Phys. Lett.* **2014**, *104*, 113501.

(12) Ghaffarzadeh, K.; Nathan, A.; Robertson, J.; Kim, S.; Jeon, S.; Kim, C.; Chung, U. I.; Lee, J. H. Persistent photoconductivity in Hf−In−Zn−O thin film transistors. *Appl. Phys. Lett.* **2010**, *97*, 143510.

(13) Jeon, S.; Ahn, S. E.; Song, I.; Kim, C. J.; Chung, U. I.; Lee, E.; Yoo, I.; Nathan, A.; Lee, S.; Robertson, J. Gated three-terminal device architecture to eliminate persistent photoconductivity in oxide semiconductor photosensor arrays. *Nat. Mater.* **2012**, *11*, 301.

(14) Standard for definitions, symbols and characteristics of floating gate memory arrays. *IEEE Standard*; 1998; DOI: 10.1109/IEEESTD.1998.89425.

(15) Jiang, H. X.; Lin, J. Y. Persistent photoconductivity and related critical phenomena in $Zn_{0.3}Cd_{0.7}Se$. *Phys. Rev. B: Condens. Matter Mater. Phys.* **1989**, *40*, 10025.

(16) Lang, D. V.; Logan, R. A.; Joros, M. Trapping characteristics and a donor-complex (DX) model for the persistent-photoconductivity trapping center in Te-doped $Al_xGa_{1-x}As$. *Phys. Rev. B* **1979**, *19*, 1015.

(17) Queisser, H. J.; Theodorou, D. E. Decay kinetics of persistent photoconductivity in semiconductors. *Phys. Rev. B: Condens. Matter Mater. Phys.* **1986**, *33*, 4027.

(18) Chen, H. M.; Chen, Y. F.; Lee, M. C.; Feng, M. S. Persistent photoconductivity in *n*-type GaN. *J. Appl. Phys.* **1997**, *82*, 899.

(19) Lin, T. Y.; Chen, H. M.; Tsai, M. S.; Chen, Y. F.; Fang, F. F.; Lin, C. F.; Chi, G. C. Two-dimensional electron gas and persistent photoconductivity in $Al_xGa_{1-x}N$/GaN heterostructures. *Phys. Rev. B: Condens. Matter Mater. Phys.* **1998**, *58*, 13793.

(20) Lin, T. Y.; Yang, H. C.; Chen, Y. F. Optical quenching of the photoconductivity in *n*-type GaN. *J. Appl. Phys.* **2000**, *87*, 3404.

DOI: 10.1021/acsphotonics.5b00084
ACS Photonics 2015, 2, 1057−1064

(21) Tarun, M. C.; Selim, F. A.; McCluskey, M. D. Persistent photoconductivity in strontium titanate. *Phys. Rev. Lett.* **2013**, *111*, 187403.
(22) Tebano, A.; Fabbri, E.; Pergolesi, D.; Balestrino, G.; Traversa, E. Room-temperature giant persistent photoconductivity in $SrTiO_3$/$LaAlO_3$ heterostructures. *ACS Nano* **2012**, *6*, 1278−1283.
(23) Singh, V.; Joung, D.; Zhai, L.; Das, S.; Khondaker, S. I.; Seal, S. Graphene based materials: Past, present and future. *Prog. Mater. Sci.* **2011**, *56*, 1178−1271.
(24) Chang, H.; Wu, H. Graphene-based nanomaterials: synthesis, properties, and optical and optoelectronic applications. *Adv. Funct. Mater.* **2013**, *23*, 1984−1997.
(25) Eda, G.; Chhowalla, M. Graphene-based composite thin films for electronics. *Nano Lett.* **2009**, *9*, 814−818.
(26) Liscio, A.; Veronese, G. P.; Treossi, E.; Suriano, F.; Rossella, F.; Bellani, V.; Rizzoli, R.; Samorı, P.; Palermo, V. Charge transport in graphene− polythiophene blends as studied by Kelvin probe force microscopy and transistor characterization. *J. Mater. Chem.* **2011**, *21*, 2924−2931.
(27) Yang, N.; Zhai, J.; Wang, D.; Chen, Y.; Jiang, L. Two-dimensional graphene bridges enhanced photoinduced charge transport in dye-sensitized solar cells. *ACS Nano* **2010**, *4*, 887−894.
(28) Lin, P.; Choy, W. C. H.; Zhang, D.; Xie, F.; Xin, J.; Leung, C. W. Semitransparent organic solar cells with hybrid monolayer graphene/metal grid as top electrodes. *Appl. Phys. Lett.* **2013**, *102*, 113303.
(29) Yang, H.; Guai, G. H.; Guo, C.; Song, Q.; Jiang, S. P.; Wang, Y.; Zhang, W.; Li, C. M. NiO/graphene composite for enhanced charge separation and collection in p-type dye sensitized solar cell. *J. Phys. Chem. C* **2011**, *115*, 12209−12215.
(30) Paton, K. R.; Varrla, E.; Backes, C.; Smith, R. J.; Khan, U.; O'Neill, A.; Boland, C.; Lotya, M.; Istrate, O. M.; King, P.; Higgins, T.; Barwich, S.; May, P.; Puczkarski, P.; Ahmed, I.; Moebius, M.; Pettersson, H.; Long, E.; Coelho, J.; O'Brien, S. E.; McGuire, E. K.; Sanchez, B. M.; Duesberg, G. S.; McEvoy, N.; Pennycook, T. J.; Downing, C.; Crossley, A.; Nicolosi, V.; Coleman, J. N. Scalable production of large quantities of defect-free few-layer graphene by shear exfoliation in liquids. *Nat. Mater.* **2014**, *13*, 624.
(31) Dai, M. K.; Lian, J. T.; Lin, T. Y.; Chen, Y. F. High-performance transparent and flexible inorganic thin film transistors: a facile integration of graphene nanosheets and amorphous InGaZnO. *J. Mater. Chem. C* **2013**, *1*, 5064−5071.
(32) Bruder, F. K.; Hagen, R.; Rölle, T.; Weiser, M. S.; Fäcke, T. From the surface to volume: concepts for the next generation of optical−holographic data-storage materials. *Angew. Chem., Int. Ed.* **2011**, *50*, 4552−4573.
(33) Hernandez, Y.; Nicolosi, V.; Lotya, M.; Blighe, F. M.; Sun, Z.; De, S.; McGovern, I. T.; Holland, B.; Byrne, M.; Gun'Ko, Y. K.; Boland, J. J.; Niraj, P.; Duesberg, G.; Krishnamurthy, S.; Goodhue, R.; Hutchison, J.; Scardaci, V.; Ferrari, A. C.; Coleman, J. N. High-yield production of graphene by liquid-phase exfoliation of graphite. *Nat. Nanotechnol.* **2008**, *3*, 563−568.
(34) Lotya, M.; Hernandez, Y.; King, P. J.; Smith, R. J.; Nicolosi, V.; Karlsson, L. S.; Blighe, F. M.; De, S.; Wang, Z.; McGovern, I. T.; Duesberg, G. S.; Coleman, J. N. Liquid phase production of graphene by exfoliation of graphite in surfactant/water solutions. *J. Am. Chem. Soc.* **2009**, *131*, 3611−3620.
(35) Ferrari, A. C.; Robertson, J. Interpretation of raman spectra of disordered and amorphous carbon. *Phys. Rev. B: Condens. Matter Mater. Phys.* **2000**, *61*, 14095−14107.
(36) Tsurumi, J.; Saito, Y.; Verma, P. Evaluation of the interlayer interactions of few layers of graphene. *Chem. Phys. Lett.* **2013**, *557*, 114−117.
(37) Ferrari, A. C.; Meyer, J. C.; Scardaci, V.; Casiraghi, C.; Lazzeri, M.; Mauri, F.; Piscanec, S.; Jiang, D.; Novoselov, K. S.; Roth, S.; Geim, A. K. Raman spectrum of graphene and graphene layers. *Phys. Rev. Lett.* **2006**, *97*, 187401.
(38) Lee, K. W.; Heo, K. Y.; Kim, H. J. Photosensitivity of solution-based indium gallium zinc oxide single-walled carbon nanotubes blend thin film transistors. *Appl. Phys. Lett.* **2009**, *94*, 102112.
(39) Street, R. A.; Ng, T.; Lujan, R. A.; Son, I.; Smith, M. J.; Kim, S.; Lee, T. Sol−gel solution-deposited InGaZnO thin film transistors. *ACS Appl. Mater. Interfaces* **2014**, *6*, 4428−4437.
(40) Nomura, K.; Ohta, H.; Takagi, A.; Kamiya, T.; Hirano, M.; Hosono, H. Room-temperature fabrication of transparent flexible thin-film transistors using amorphous oxide semiconductors. *Nature* **2004**, *432*, 488.
(41) Park, S. H. K.; Ryu, M. K.; Yoon, S. M.; Yang, S.; Hwang, C. S.; Jeon, J. H. Device reliability under electrical stress and photo response of oxide TFTs. *J. Soc. Inf. Disp.* **2010**, *18*, 779−788.
(42) Ryu, B.; Noh, H. K.; Choi, E. A.; Chang, K. J. O-vacancy as the origin of negative bias illumination stress instability in amorphous In−Ga−Zn−O thin film transistors. *Appl. Phys. Lett.* **2010**, *97*, 022108.
(43) Ghaffarzadeh, K.; Nathan, A.; Robertson, J.; Kim, S.; Jeon, S.; Kim, C.; Chung, U. I.; Lee, J. H. Instability in threshold voltage and subthreshold behavior in Hf−In−Zn−O thin film transistors induced by bias-and light-stress. *Appl. Phys. Lett.* **2010**, *97*, 113504.
(44) Görrn, P.; Lehnhardt, M.; Riedl, T.; Kowalsky, W. The influence of visible light on transparent zinc tin oxide thin film transistors. *Appl. Phys. Lett.* **2007**, *91*, 193504.
(45) Peng, L.; Hu, L. F.; Fang, X. S. Energy harvesting for nanostructured self-powered photodetectors. *Adv. Funct. Mater.* **2014**, *24*, 2591−2610.
(46) Chang, H.; Sun, Z.; Ho, K. Y. F.; Tao, X.; Yan, F.; Kwok, W. M.; Zheng, Z. A highly sensitive ultraviolet sensor based on a facile in situ solution-grown ZnO nanorod/graphene heterostructure. *Nanoscale* **2011**, *3*, 258.
(47) Liu, X. Q.; Liu, X.; Wang, J. L.; Liao, C. N.; Xiao, X. H.; Guo, S. S.; Jiang, C. Z.; Fan, Z. Y.; Wang, Ti.; Chen, X. S.; Lu, W.; Hu, W. D.; Liao, L. Transparent, high-performance thin-film transistors with an InGaZnO/aligned-SnO_2-nanowire composite and their application in photodetectors. *Adv. Mater.* **2014**, *26*, 7399−7404.
(48) Chiu, C. J.; Weng, W. Y.; Chang, S. J.; Chang, S. P.; Chang, T. H. A deep UV sensitive Ta_2O_5/a-IGZO TFT. *IEEE Sens. J.* **2011**, *11*, 2902−2905.
(49) Lee, K. W.; Kim, K. M.; Heo, K. Y.; Park, S. K.; Lee, S. K.; Kim, H. J. Effects of UV light and carbon nanotube dopant on solution-based indium gallium zinc oxide thin-film transistors. *Curr. Appl. Phys.* **2011**, *11*, 280−285.
(50) Takechi, K.; Nakata, M.; Eguchi, T.; Yamaguchi, H.; Kaneko, S. Comparison of ultraviolet photo-field effects between hydrogenated amorphous silicon and amorphous InGaZnO4 thin-film transistors. *Jpn. J. Appl. Phys.* **2009**, *48*, 010203.
(51) Chowdhury, M. D. H.; Migliorato, P.; Jang, J. Light induced instabilities in amorphous indium−gallium−zinc−oxide thin-film transistors. *Appl. Phys. Lett.* **2010**, *97*, 173506.
(52) Chen, W. T.; Hsueh, H. W.; Zan, H. W.; Tsai, C. C. Light-enhanced bias stress effect on amorphous In-Ga-Zn-O thin-film transistor with lights of varying colors. *Electrochem. Solid-State Lett.* **2011**, *14*, H297−H299.
(53) Ujimoto, M.; Takashima, W.; Kaneto, K. Photo induced memory devices using conducting polymer, poly(3-hexylthiophene) thin films. *Thin Solid Films* **2006**, *499*, 313−317.
(54) Lu, M. P.; Lu, M. Y.; Chen, L. J. Multibit Programmable Optoelectronic Nanowire Memory with Sub-femtojoule Optical Writing Energy. *Adv. Funct. Mater.* **2014**, *24*, 2967−2974.
(55) Liu, X. H.; Zhao, H. Y.; Dong, G. F.; Duan, L.; Li, D.; Wang, L. D.; Qiu, Y. Multifunctional organic phototransistor-based nonvolatile memory achieved by UV/ozone treatment of the Ta_2O_5 gate dielectric. *ACS Appl. Mater. Interfaces* **2014**, *6*, 8337−8344.

DOI: 10.1021/acsphotonics.5b00084
ACS Photonics 2015, 2, 1057−1064